

# Near-Heisenberg-limited parallel amplitude estimation with logarithmic depth circuit

Kohei Oshio,<sup>1, 2,\*</sup> Kaito Wada,<sup>3, †</sup> and Naoki Yamamoto<sup>2, 4, ‡</sup>

<sup>1</sup>*Mizuho Research & Technologies, Ltd., 2-3, Kandanishiki, Chiyoda-ku, Tokyo, 100-8233, Japan*

<sup>2</sup>*Quantum Computing Center, Keio University, 3-14-1 Hiyoshi, Kohoku-ku, Yokohama, Kanagawa, 223-8522, Japan*

<sup>3</sup>*Graduate School of Science and Technology, Keio University, 3-14-1 Hiyoshi, Kohoku, Yokohama, Kanagawa 223-8522, Japan*

<sup>4</sup>*Department of Applied Physics and Physico-Informatics, Keio University, Hiyoshi 3-14-1, Kohoku-ku, Yokohama 223-8522, Japan*

Quantum amplitude estimation is one of the core subroutines in quantum algorithms. This paper gives a parallelized amplitude estimation (PAE) algorithm, that simultaneously achieves near-Heisenberg scaling in the total number of queries and sub-linear scaling in the circuit depth, with respect to the estimation precision. The algorithm is composed of a global GHZ state followed by separated low-depth Grover circuits; the number of qubits in the GHZ state and the depth of each circuit is tunable as a trade-off way, which particularly enables even near-Heisenberg-limited and logarithmic-depth algorithm for amplitude estimation. The quantum signal processing technique is effectively used to build the algorithm. The proposed algorithm has a form of distributed quantum computing, which may be suitable for device implementation.

*Introduction.*— Estimating unknown parameters in quantum systems is a central topic in quantum metrology [1, 2]. Many efficient estimation strategies have been developed in various settings; in particular, two major strategies toward quantum-limited estimation are the *parallel* and *sequential strategies*, which roughly speaking, utilize a large entanglement and a long coherence-time, respectively. The techniques in quantum metrology are powerful, and there has been growing interest in applying such techniques to the development of efficient algorithms for quantum computation scenario [3–11].

In those estimation algorithms, Quantum Amplitude Estimation (QAE) [12] is an essential component. Because it can be applied to mean-value estimation for any observable, it has numerous applications such as chemistry [13–16], finance [17–19], and machine learning [20–23]. Specifically, in QAE, we are given an  $n$ -qubit ( $n \geq 2$ ) unitary operator  $U_a$  (and  $U_a^\dagger$ ) that encodes the target amplitude  $a \in [0, 1]$  as

$$U_a |0\rangle^{\otimes n} = \sqrt{1-a} |\psi_0\rangle |0\rangle + \sqrt{a} |\psi_1\rangle |1\rangle, \quad (1)$$

where  $|\psi_0\rangle$  and  $|\psi_1\rangle$  are unknown  $(n-1)$ -qubit quantum states. The goal is to estimate the amplitude  $a$  by measuring the output state of single or multiple quantum circuits that contains  $U_a$  and  $U_a^\dagger$ . The performance of the QAE algorithm is evaluated by the relationship between the root mean squared estimation error (RMSE)  $\varepsilon$  and the total number  $N$  of queries to  $U_a$  and  $U_a^\dagger$  in the whole procedure. Notably, the conventional QAE methods [24–29] achieve the Heisenberg-limited (HL) scaling  $N = \mathcal{O}(1/\varepsilon)$  or the near-HL one  $N = \tilde{\mathcal{O}}(1/\varepsilon)$  (where  $\tilde{\mathcal{O}}$

suppresses logarithmic factors), over the classical scaling  $\mathcal{O}(1/\varepsilon^2)$ . However, those QAE methods require applying  $U_a$  and  $U_a^\dagger$  sequentially on a single circuit, which consequently causes the maximal circuit depth to scale as  $\mathcal{O}(1/\varepsilon)$ .

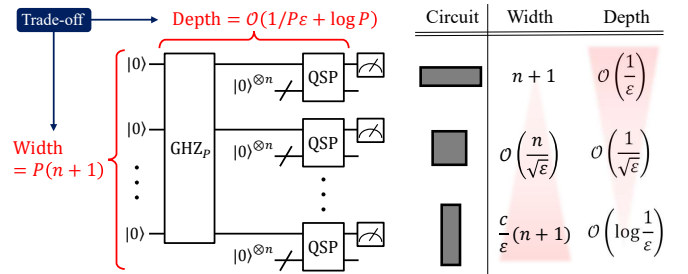


FIG. 1. Quantum circuit of PAE, where  $P \in [1, c/\varepsilon]$  represents the factor of parallelization with  $c$  a constant. “Width” denotes the total number of qubits.  $P$  is tuned to control the trade-off between total qubits and depth, as shown in several cases; Theorem 1 in Introduction states the extreme log-depth case with  $P = [1/\varepsilon]$ . The  $\text{GHZ}_P$  operator prepares a  $P$ -qubit GHZ state,  $(|0\rangle^{\otimes P} + |1\rangle^{\otimes P})/\sqrt{2}$ . The QSP operator denotes an engineered phase shifter constructed by quantum signal processing (QSP), represented as  $V_{\varphi,T}$  in the main text.

Reducing the circuit depth even at the expense of increasing the number of qubits is often an effective approach to make quantum circuits easier to implement, which is thus a central paradigm in quantum algorithm synthesis [30–38]. For instance, quantum signal processing (QSP) for specific problems can be parallelized using multiple systems, enabling the linear depth reduction with respect to the number of systems employed [36]. Another recent result is that the circuit for approximating random unitaries can be exponentially reduced in depth by adding ancilla qubits [38]. However, for the QAE problem, there exists only a few approaches to take this

\* [kohei.oshio@quantum.keio.ac.jp](mailto:kohei.oshio@quantum.keio.ac.jp)

† [wkai1013keio840@keio.jp](mailto:wkai1013keio840@keio.jp); K.O. and K.W. contributed equally to this work.

‡ [yamamoto@appi.keio.ac.jp](mailto:yamamoto@appi.keio.ac.jp)

direction [39–41]. Refs. [39, 41] provide an example that achieves a depth of  $\mathcal{O}(1/\varepsilon^{1-\kappa})$  with some constant  $\kappa$ , but it requires the total queries of  $\tilde{\mathcal{O}}(1/\varepsilon^{1+\kappa})$ , which is strictly bigger than the near HL scaling. Overall, there has been no QAE algorithm achieving  $N = \tilde{\mathcal{O}}(1/\varepsilon)$  for any  $a \in [0, 1]$  with the use of quantum circuits whose maximal depth is sublinear in  $1/\varepsilon$ . In particular, there has been no log-depth QAE algorithm that achieves  $N = \tilde{\mathcal{O}}(1/\varepsilon)$ .

Intuitively, applying the quantum metrological parallel strategy to the QAE setting might work to solve the above-mentioned problems, especially given that the Grover operator  $Q$  in the QAE algorithms is a rotation gate with the angle  $2 \arcsin \sqrt{a}$ . However, there is a tough obstacle; in the QAE problem, the eigenstates of  $Q$  are not generally accessible unlike the conventional metrology setting, implying that the phase kick-back (from the system to the probe system prepared in e.g., GHZ state) technique cannot be directly applied.

In this paper, we apply the QSP [42] to overcome this issue, thereby presenting a new QAE algorithm—parallel amplitude estimation (PAE)—that achieves the desirable scaling in both the queries and the circuit depth; the following theorem is a special case achieving the log-depth circuit.

**Theorem 1** (Parallel amplitude estimation; log-depth case). *Let  $\varepsilon \in (0, 1)$ . There exists a quantum algorithm that estimates the amplitude  $a \in [0, 1]$  encoded in  $U_a$  within the RMSE  $\varepsilon$ , using  $N = \mathcal{O}(\varepsilon^{-1} \log(1/\varepsilon))$  queries to  $U_a$  and  $U_a^\dagger$  in total and  $\lceil 1/\varepsilon \rceil (n + 1)$ -qubit quantum circuits with circuit depth of  $\mathcal{O}(\log(1/\varepsilon))$ .*

That is, PAE resolves the above-mentioned open problem; PAE can achieve the near HL scaling,  $N = \tilde{\mathcal{O}}(1/\varepsilon)$ , using quantum circuits with exponentially shallow depth  $\mathcal{O}(\log(1/\varepsilon))$  for the target RMSE  $\varepsilon$ . Hereafter, we refer to the number of sequential applications of  $U_a$  (and  $U_a^\dagger$ ) on a single circuit as the “circuit depth”.

Theorem 1 can be generalized (the statement will be shown later), and Fig. 1 depicts the circuit of that general PAE algorithm. The parallelization factor  $P$  in the total qubit count can be chosen to take any integer in  $1 \leq P \leq c/\varepsilon$  with  $c$  a constant. The above Theorem 1 states the extreme log-depth case with  $P = \lceil 1/\varepsilon \rceil$ . This notable parallel structure in Fig. 1 indeed comes from the parallel strategy in quantum metrology; how to resolve the above-mentioned phase kick-back issue via QSP to realize this parallel structure will be discussed later. The degree of freedom of  $P$  is a key feature of PAE, which can be chosen depending on the quality of hardware; if a longer circuit depth is allowed, for instance we may take  $P = 1/\sqrt{\varepsilon}$ , in which case the circuit depth increases to  $\mathcal{O}(1/\sqrt{\varepsilon})$  and the number of qubits is reduced to  $\mathcal{O}(n/\sqrt{\varepsilon})$ . Another apparently important feature of PAE is that a (large) entanglement between multiple qubits is needed only at the beginning of the circuit, and after this, the circuit has a completely separable structure including the final measurement. This indicates that our method can be executed in parallel using multiple

$\mathcal{O}(n)$ -qubit quantum computers with a pre-shared entangled state. Moreover, the pre-shared entangled state is given by a  $P$ -qubit GHZ state  $(|0\rangle^{\otimes P} + |1\rangle^{\otimes P})/\sqrt{2}$ , which can be generated in quantum circuits with a logarithmic depth in  $P$  [43, 44]. For these reasons, our method is suitable for device implementation, especially in a form of distributed quantum computing [45–50]. We compare PAE and conventional QAE [12, 24, 25, 39] in terms of the circuit depth, the total qubits count, and the query complexity; a summary of this comparison is provided in the table presented in Supplemental Material Sec. S1.

*Parallel strategy in quantum metrology.*— The standard problem addressed by the parallel strategy [1] is the estimation of an unknown phase  $\varphi$  embedded in a unitary operator  $U_\varphi := e^{i\varphi H}$ . The crucial assumption is that the corresponding eigenstate of Hamiltonian  $H$  can be prepared, i.e.,  $U_\varphi |\varphi\rangle = e^{i\varphi} |\varphi\rangle$ . A canonical procedure of the parallel strategy is that we first prepare a  $P$ -qubit GHZ state  $|\text{GHZ}_P\rangle = (|0\rangle^{\otimes P} + |1\rangle^{\otimes P})/\sqrt{2}$  together with  $|\varphi\rangle^{\otimes P}$  and then apply the controlled-unitary  $cU_\varphi = |0\rangle\langle 0| \otimes I + |1\rangle\langle 1| \otimes U_\varphi$  in parallel:

$$cU_\varphi^{\otimes P} |\text{GHZ}_P\rangle |\varphi\rangle^{\otimes P} = \frac{|0\rangle^{\otimes P} + e^{iP\varphi} |1\rangle^{\otimes P}}{\sqrt{2}} |\varphi\rangle^{\otimes P}. \quad (2)$$

Thus, the phase  $\varphi$  is effectively kick-backed with multiplicative factor  $P$ , enabling the quantum-enhanced estimation of  $\varphi$  to achieve the HL scaling in  $P$  [1]. Note again that the above operation is doable if  $|\varphi\rangle$  is available, while, if not, the possibility of doing a similar phase kick-back technique is non-trivial. This is the main reason why the direct application of the parallel strategy to the QAE problem is a significant challenge. Below we describe this fact in detail.

*Challenges of the parallel strategy for amplitude estimation.*— In the QAE problem, the following Grover operator has an important role:

$$Q := U_0 U_a^\dagger U_f U_a, \quad (3)$$

where  $U_0 := 2|0\rangle^{\otimes n} \langle 0| - I^{\otimes n}$ ,  $U_f := 2I^{\otimes n-1} \otimes |0\rangle\langle 0| - I^{\otimes n}$ , and  $I$  is an identity operator.  $Q$  acts as  $Q|0\rangle^{\otimes n} = \cos 2\theta |0\rangle^{\otimes n} + \sin 2\theta |\psi\rangle$ , where  $\theta := \arcsin \sqrt{a}$  and  $|\psi\rangle$  is a quantum state orthogonal to  $|0\rangle^{\otimes n}$  [51, 52]. In the subspace spanned by  $|0\rangle^{\otimes n}$  and  $|\psi\rangle$ , called “Grover plane”,  $Q$  functions as a rotation  $e^{-i2\theta \bar{Y}}$  for the Pauli  $\bar{Y}$  defined in this subspace.  $Q$  has the eigenstates  $|Q_\pm\rangle := (|0\rangle^{\otimes n} \pm i|\psi\rangle)/\sqrt{2}$ , which satisfy

$$Q|Q_\pm\rangle = e^{\mp 2i\theta} |Q_\pm\rangle. \quad (4)$$

Toward realizing the parallel strategy for the QAE problem, we consider the controlled Grover operator  $cQ := |0\rangle\langle 0|_b \otimes I_s + |1\rangle\langle 1|_b \otimes Q$ , where  $b$  and  $s$  are indices corresponding to the ancilla qubit and the  $n$ -qubit system. If the input state  $|\text{GHZ}_P\rangle_b \otimes |Q_\sigma\rangle_s^{\otimes P}$  with  $\sigma = +$  or  $\sigma = -$  can be prepared, a signal multiplication operation similar to Eq. (2) can be realized by applying  $cQ^{\otimes P}$  to

this input state. However, in the QAE problem, only the black-box operation  $Q$  (or  $U_a$  and  $U_a^\dagger$ ) is given, and the eigenstates  $|Q_\pm\rangle$  are generally unknown, meaning that the phase kick-back technique with  $cQ$  cannot be directly applied to enhanced the signal. There are two previous approaches; one is to prepare  $|Q_\pm\rangle$  under the assumption of a sufficiently large amplitude [3], and the other generates a particularly structured  $|Q_\pm\rangle$  [53]. Unlike these approaches, we design a general and efficient parallel estimation method that works for arbitrary  $a \in [0, 1]$  and black boxes  $U_a, U_a^\dagger$ , as described below.

*Parallelization by QSP.*— To overcome the difficulty in preparing unknown states, we convert  $cQ$  into an engineered phase shifter which encodes the target parameter  $a$  into the relative phase between *known* eigenstates. The key idea of our approach is to make the eigenphases of  $Q$  degenerate in the Grover plane; note that a similar technique has been employed in Ref. [42, 51] in other problem settings. Now,  $cQ$  can be expressed as

$$cQ = \sum_{\sigma} e^{-i\sigma\theta} \begin{pmatrix} e^{i\sigma\theta} & 0 \\ 0 & e^{-i\sigma\theta} \end{pmatrix}_b \otimes |Q_\sigma\rangle\langle Q_\sigma|_s$$

where  $\sigma \in \{+, -\}$  and we omit terms acting outside the Grover plane. Suppose we have an operation to transform the eigenphases  $\sigma\theta$  to  $h(\sigma\theta) = -T \cos(2\sigma\theta)$  and remove the global phase; then  $cQ$  is transformed to

$$\begin{aligned} & \sum_{\sigma} \begin{pmatrix} e^{-iT \cos(2\sigma\theta)} & 0 \\ 0 & e^{iT \cos(2\sigma\theta)} \end{pmatrix}_b \otimes |Q_\sigma\rangle\langle Q_\sigma|_s \\ &= \begin{pmatrix} e^{-iT\varphi/2} & 0 \\ 0 & e^{iT\varphi/2} \end{pmatrix}_b \otimes \sum_{\sigma} |Q_\sigma\rangle\langle Q_\sigma|_s \end{aligned}$$

where  $T$  represents some time duration and  $\varphi = 2 \cos 2\theta = 2(1 - 2a)$ . Hence, this procedure results in the following transformation:

$$cQ \mapsto \tilde{V}_{\varphi,T} := \begin{pmatrix} e^{-iT\varphi/2} & 0 \\ 0 & e^{iT\varphi/2} \end{pmatrix}_b \otimes \bar{I}_s, \quad (5)$$

where  $\bar{I}_s$  is the identity operator on the Grover plane, and terms acting outside the Grover plane are omitted. Consequently, after separately preparing an arbitrary state, particularly *known* state such as  $|0\rangle_s^{\otimes n}$  on the Grover plane, the resulting operation acts as the relative phase shifter of  $T\varphi$  for any state in  $b$ .

We can approximately achieve the above procedure using QSP [42, 54, 55], which is a general technique for applying polynomial transformations to the eigenvalues of a given operator. In our setting, the target operator is  $Q$ , and we focus only on the eigenvalues of  $|Q_\pm\rangle$ , whereas QSP transforms all eigenvalues. A brief overview on how to construct  $V_{\varphi,T}$  is given in Appendix A, with a full exposition provided in Supplemental Material Sec. S2. To quantify the resource requirements for this transformation, we introduce the following Lemma 1:

**Lemma 1** (Query complexity for constructing  $V_{\varphi,T}$ ).  
For any oracle conversion error  $\varepsilon_{\text{oc}} \in (0, 1)$  and any  $j \in \{0, 1\}$ , there exists a quantum algorithm that constructs an operator  $V_{\varphi,T}$  such that

$$\left\| \left( V_{\varphi,T} - \tilde{V}_{\varphi,T} \right) |j\rangle_b |0\rangle_s^{\otimes n} \right\| < \varepsilon_{\text{oc}},$$

using  $cQ$  and  $cQ^\dagger$  a total of  $L = \mathcal{O}(T + \log(1/\varepsilon_{\text{oc}}))$  times.

Lemma 1 can be derived by applying the theory of QSP developed in prior works [42, 51, 56] to this operator transformation; the detailed proof is given in Supplemental Material Sec. S3. Since  $cQ$  consists of one  $U_a$  and one  $U_a^\dagger$  as depicted in Appendix A Fig. 3, we can achieve an approximation error of  $\varepsilon_{\text{oc}}$  with logarithmic number of (control-free) operations of  $U_a$  and  $U_a^\dagger$ . As a result, this cost accounts for the additional  $\log(1/\varepsilon)$  factor in the query complexity stated in Theorem 1.

With  $V_{\varphi,T}$ , we can perform a similar amplification to Eq. (2):

$$\begin{aligned} |\Psi(M = PT)\rangle &:= V_{\varphi,T}^{\otimes P} |\text{GHZ}_P\rangle_b |0\rangle_s^{\otimes nP} \\ &\approx \frac{e^{-iM\varphi/2} |0\rangle_b^{\otimes P} + e^{iM\varphi/2} |1\rangle_b^{\otimes P}}{\sqrt{2}} \otimes |0\rangle_s^{\otimes nP}, \quad (6) \end{aligned}$$

where  $|\text{GHZ}_P\rangle_b := (|0\rangle_b^{\otimes P} + |1\rangle_b^{\otimes P})/\sqrt{2}$ . That is, the phase  $\varphi$  is successfully kick backed to the ancilla space with multiplicative enhancement factor  $M = PT$ . Again, this is the transformation on the Grover plane. Also note that  $|0\rangle_s^{\otimes nP}$  can now be prepared without knowing  $|Q_\pm\rangle$ . The quantum circuit for this operation is illustrated in Fig. 1, where the QSP operator denotes  $V_{\varphi,T}$ . Note that for a given  $M$ , the parameters  $P$  and  $T$  are chosen according to the available quantum resources.

*Amplitude estimation with parallel strategy.*— In PAE, we estimate  $\varphi = 2(1 - 2a)$ , approximately embedded in  $V_{\varphi,T}$ . Specifically, to establish the estimation procedure without any ambiguity, we leverage the robust phase estimation (RPE) method [4, 57] through the following quantum-enhanced measurement in the parallel strategy. The concrete procedure for estimating  $\varphi$  using RPE is as follows. Let  $K$  be some positive integer. (i) For each  $k \in \{1, 2, \dots, K\}$ , prepare  $|\Psi(M_k = 2^{k-1})\rangle$  with an arbitrary pair  $(P_k, T_k)$  such that  $P_k T_k = 2^{k-1}$ . Then perform each of the two projective measurements including the bases  $\{|\pm P_k\rangle_b := (|0\rangle_b^{\otimes P_k} \pm |1\rangle_b^{\otimes P_k})/\sqrt{2}\}$  or  $\{|\pm i P_k\rangle_b := (|0\rangle_b^{\otimes P_k} \pm i |1\rangle_b^{\otimes P_k})/\sqrt{2}\}$  on the ancilla subsystem  $\nu_k$  times, and record the number of trials in which the outcomes are  $|+ P_k\rangle_b$  and  $|i P_k\rangle_b$ , respectively. (ii) Conduct classical postprocessing on the results of (i) to estimate the phase. The pseudocode for the classical post-processing in (ii) is presented in Appendix B, while further details are presented in Supplemental Material Sec. S4. This post-processing is very simple and its computational cost is almost negligible.

Notably, the outcomes of the two projective measurements in (i) can be reproduced by measuring each ancilla

qubit [58]. The probability of obtaining an even number of 1s from X-measurements on the ancilla qubits of  $|\Psi(M_k)\rangle$  equals the projection probability onto  $|+_P\rangle_b$ . After applying  $e^{i\pi Z/4}$  to the first ancilla qubit, the probability corresponds to that of finding  $|+_P\rangle_b$ . Therefore, in PAE, the only quantum operation across  $P$  parallel systems is the preparation of  $|\text{GHZ}_P\rangle_b$ . In addition, since all the  $k$ -th processes in (i) are independent, they can be executed in parallel. The pseudocode of PAE is provided in Appendix B.

Importantly, the RPE procedure works well even if the quantum state preparation and/or measurement contain some small errors. Here, we assume that the probabilities of obtaining the outcomes corresponding to projective measurements onto  $|+_P\rangle_b$  and  $|i_P\rangle_b$  are given by  $p_{+,k} := (1 + \cos M_k \varphi)/2 + \beta_{+,k}$  and  $p_{i,k} := (1 + \sin M_k \varphi)/2 + \beta_{i,k}$ , respectively, where  $\beta_{r,k}$  (for  $r \in \{+, i\}$ ) denotes the bias in the measurement probability caused by the approximation error of  $V_{\varphi,T}$  or the computational error. Due to the robustness of RPE, one can achieve the HL scaling for the estimation of  $\varphi$  if  $|\beta_{r,k}| < \sqrt{6}/8$  [4, 58]. Based on the discussion in Ref. [58], we have the following lemma regarding  $\beta_{r,k}$  and the mean squared estimation error (MSE) upper bound:

**Lemma 2** (MSE upper bound of RPE [58]). *Suppose the measurement bias parameters  $\{\beta_{r,k}\}$  satisfy  $\sup_{r,k} \{|\beta_{r,k}|\} := \beta < \sqrt{6}/8$ . Then, the RPE procedure (i)–(ii) returns the phase estimate  $\hat{\varphi} \in (-\pi, \pi]$  such that its mean squared error (MSE) satisfies*

$$\mathbb{E}[(\hat{\varphi} - \varphi)^2] \leq \left(\frac{2\pi}{3}\right)^2 \left( \frac{1}{4^K} + \sum_{k=1}^K \frac{e^{-2\nu_k(\sqrt{6}/8 - \beta)^2}}{4^{k-4}} \right). \quad (7)$$

We now provide Theorem 1 for the general case of  $P$ , followed by the proof.

**Theorem 1** (Parallel amplitude estimation; general case). *Let  $\varepsilon \in (0, 1)$ , and let  $P$  be any positive integer. There exists a quantum algorithm that estimates the amplitude  $a \in [0, 1]$  encoded in  $U_a$  (Eq. (1)) within the RMSE  $\varepsilon$ , using  $N = \mathcal{O}(1/\varepsilon + P \log P)$  queries to  $U_a$  and  $U_a^\dagger$  in the whole procedure. This quantum algorithm uses  $P(n+1)$ -qubit quantum circuits with the structure depicted in Fig. 1 and the circuit depth of  $\mathcal{O}(1/\varepsilon P + \log P)$ .*

*Proof of Theorem 1.*— The goal is, in the framework of RPE, to compute the necessary resources (circuit depth and width) such that the right hand side of Eq. (7) in Lemma 2 is at most  $\varepsilon^2$ . The condition in this Lemma on the measurement bias,  $|\beta_{r,k}| < \beta$ , is related to the approximation error of  $V_{\varphi,T}$ , which allows us to identify the necessary circuit depth from Lemma 1. Hence, let us begin with evaluating the state error.

When  $V_{\varphi,T_k}$  is applied in parallel to  $P_k$  systems in the

same manner as Fig. 1, the following inequality holds:

$$\begin{aligned} & \left\| \left( V_{\varphi,T_k}^{\otimes P_k} - \tilde{V}_{\varphi,T_k}^{\otimes P_k} \right) |\text{GHZ}_{P_k}\rangle_b |0\rangle_s^{\otimes n P_k} \right\| \\ & \leq \sqrt{2} \max_{j=0,1} \left\| \left( V_{\varphi,T_k}^{\otimes P_k} - \tilde{V}_{\varphi,T_k}^{\otimes P_k} \right) |j\rangle_b^{\otimes P_k} |0\rangle_s^{\otimes n P_k} \right\| \\ & = \sqrt{2} P_k \max_{j=0,1} \left\| (V_{\varphi,T_k} - \tilde{V}_{\varphi,T_k}) |j\rangle_b |0\rangle_s^{\otimes n} \right\|. \end{aligned} \quad (8)$$

In addition, for  $|\tilde{\Psi}(M_k)\rangle := \tilde{V}_{\varphi,T_k}^{\otimes P_k} |\text{GHZ}_{P_k}\rangle_b |0\rangle_s^{\otimes n P_k}$  and its approximation  $|\Psi(M_k)\rangle$ , we have

$$\mathfrak{D}(|\Psi(M_k)\rangle, |\tilde{\Psi}(M_k)\rangle) \leq \|\Psi(M_k)\rangle - |\tilde{\Psi}(M_k)\rangle\|,$$

where  $\mathfrak{D}(|\Psi(M_k)\rangle, |\tilde{\Psi}(M_k)\rangle)$  is the trace distance between these states. Now, we connect this state error to the bias error  $\beta_{r,k}$  in measuring the states  $|\Psi(M_k)\rangle$  and  $|\tilde{\Psi}(M_k)\rangle$ . Specifically, from the result that the trace distance between two quantum states upper bounds the total variation distance for any POVM [59], we have  $|\beta_{r,k}| \leq \mathfrak{D}(|\Psi(M_k)\rangle, |\tilde{\Psi}(M_k)\rangle)$ . Therefore,  $|\beta_{r,k}| \leq \sqrt{2} P_k \max_j \|(V_{\varphi,T_k} - \tilde{V}_{\varphi,T_k}) |j\rangle_b |0\rangle_s^{\otimes n}\|$  holds. Meanwhile, by setting  $L_k = \mathcal{O}(T_k + \log(P_k/\beta))$  with  $\beta \in (0, \sqrt{6}/8)$  in Lemma 1, we have  $|\beta_{r,k}| < \beta$ . Hence, the MSE of  $\varphi$  is upper bounded by Eq. (7) in Lemma 2.

This leads us to choose  $K = \lceil \log_2(1/\varepsilon) \rceil + 6$  and  $\nu_k = 1 + \lceil \log 6 \times (K - k)/2(\sqrt{6}/8 - \beta)^2 \rceil$ ; then Eq. (7) gives the inequality  $\mathbb{E}[(\hat{\varphi} - \varphi)^2] < \varepsilon^2$ . Note that from  $\varphi = 2(1 - 2a)$ , we obtain  $\mathbb{E}[(\hat{a} - a)^2] \leq \mathbb{E}[(\hat{\varphi} - \varphi)^2]$  and thus  $\sqrt{\mathbb{E}[(\hat{a} - a)^2]} < \varepsilon$ . The total number of queries to the operator  $U_a$  and  $U_a^\dagger$  is given by  $N = 2 \sum_{k=1}^K \nu_k L_k P_k$ . Substituting the above  $\nu_k$  and  $L_k$ , and taking  $P_k = 1$  for all  $k$  satisfying  $2^k \leq 2^K/P$  and  $T_k = 2^{K-1}/P$  for the other  $k$ , we end up with

$$N = 2 \sum_{k=1}^K \nu_k P_k L_k = \mathcal{O}\left(\frac{1}{\varepsilon} + P \log P\right), \quad (9)$$

where we note that  $\max_k P_k \leq P$  holds.

Next, we consider the maximum depth and number of qubits. From the largest  $T_K = 2^{K-1}/P = \mathcal{O}(1/\varepsilon P)$ , we obtain  $L_K = \mathcal{O}(1/\varepsilon P + \log P)$ , and the depth of  $V_{\varphi,T_K}$  is  $\mathcal{O}(L_K)$ .  $|\text{GHZ}_P\rangle$  can be constructed from  $|0\rangle^{\otimes P}$  with the  $\log P$ -depth circuit [43, 44]. Therefore, the total depth of the circuit is  $\mathcal{O}(1/\varepsilon P + \log P)$ . Additionally, at most  $P$  instance of an  $(n+1)$ -qubit system is arranged in parallel, thus the maximum number of qubits is  $P(n+1)$ . ■

*Numerical experiment.*— We here study the total query counts and the circuit depth of PAE via numerical simulation. We set  $n = 2$  and estimate RMSE over 100 trials for  $a \in \{0, \sin^2(\pi/8)\}$  and  $K \in \{1, 2, \dots, 9\}$ . The measurement schedule  $\nu_k$  is chosen as the RPE-optimized one  $\nu_k = \lfloor 4.0835(K - k) + \nu_K \rfloor$  with  $\nu_K \in \{7, 18\}$  [58]. As for the choice of  $P_k$  and  $T_k$ , we consider the two cases: (i) *Full parallel*: fix  $T_k = 1 \forall k$  and set  $P_k = 2^{k-1}$ , and (ii) *Full sequential*: fix  $P_k = 1 \forall k$  and set  $T_k = 2^{k-1}$ .

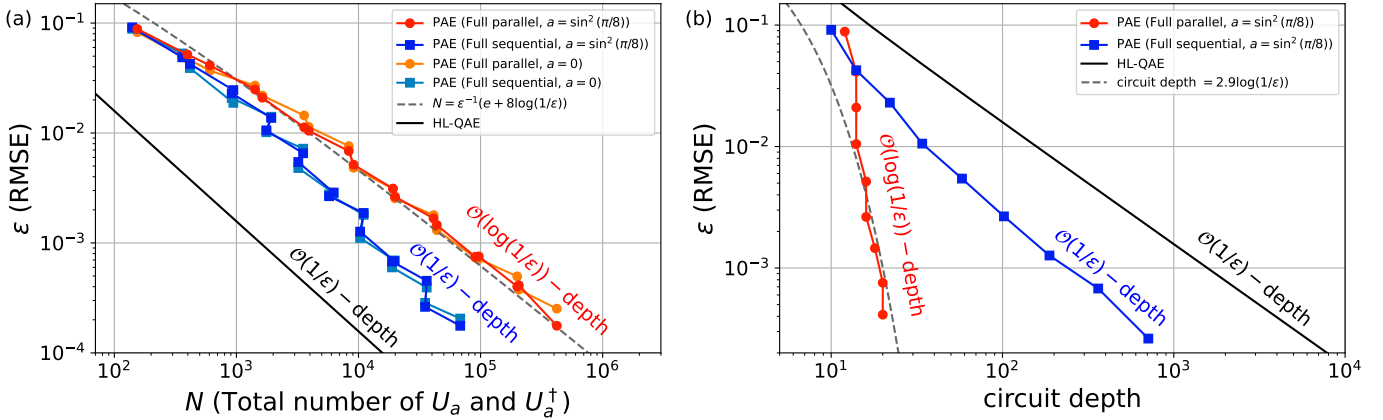


FIG. 2. (a) Relationship between the number of queries to  $U_a$  and  $U_a^\dagger$  and the estimation error (RMSE), and (b) relationships between the circuit depth and the RMSE. “Full parallel” and “Full sequential” correspond to the cases (i) and (ii), respectively. In both graphs, the gray dashed line shows a simple fitting result for the “Full parallel” case with  $a = \sin^2(\pi/8)$ .

In the case (i), we used Qiskit [60] for quantum circuit simulation and a Python library [61, 62] to compute the QSP hyperparameters. In the case (ii), the estimation is performed by sampling from the measurement distribution that assumes ideal operator transformations (i.e.,  $V_\varphi = \tilde{V}_\varphi$ ). In both cases,  $L_k$  is chosen to sufficiently suppress the approximation error in  $V_{\varphi,T}$ , ensuring that  $|\beta_{r,k}| \leq 0.05$ , as detailed in Supplemental Material Sec. S5. For comparison, we also plot the query counts of “HL-QAE” [63] ( $\varepsilon = \pi/2(N-1)$ ), which is the most query-efficient QAE proposed to date.

Figure 2(a) shows the query counts versus RMSE, for two specific target values of  $a$ . In the full sequential case (ii), PAE achieves the HL scaling  $N = \mathcal{O}(1/\varepsilon)$ . In the full parallel case (i), the scaling remains HL with logarithmic overhead,  $N = \mathcal{O}(\varepsilon^{-1}\log(1/\varepsilon))$ , consistent with Theorem 1. This overhead leads to about 4 times bigger queries  $N$  for  $\varepsilon = 10^{-3}$ , but we recall that the full parallel PAE works only with log-depth circuit. This is clearly seen in Fig. 2(b) showing the circuit depth versus RMSE. Actually, in the case (i), the depth scales logarithmically in  $1/\varepsilon$ , also in agreement with Theorem 1. On the other hand, the PAE with the case (ii) needs  $\mathcal{O}(1/\varepsilon)$  depth, which is the same as HL-QAE. Note however that, compared to HL-QAE which requires  $\mathcal{O}(\log(1/\varepsilon))$  ancilla qubits, this PAE achieves roughly 1/6 circuit depth for  $\varepsilon \lesssim 5 \times 10^{-3}$  while using only a single ancilla qubit, at the cost of about 10 times increase in  $N$  as observed in Fig. 2(a).

*Summary and discussion.*— In this paper, we proposed the PAE algorithm, which realizes the parallel strategy commonly used in the quantum metrology context, via the engineered phase shifter constructed by QSP. PAE enables us to estimate the target amplitude  $a$  with RMSE  $\varepsilon$ , with the quantum circuit of depth  $\mathcal{O}(1/P\varepsilon + \log P)$ , where  $P \in [1, c/\varepsilon]$  is a controllable parallelization factor; the total number of queries of  $U_a$  is  $N = \mathcal{O}(1/\varepsilon + P\log P)$ . This indicates that in an extreme case of  $P = \mathcal{O}(1/\varepsilon)$ , PAE achieves the HL scaling

with logarithmic overhead using  $\mathcal{O}(\log(1/\varepsilon))$ -depth circuits. We demonstrated PAE with a numerical experiment to confirm that the results are consistent with the theoretical analysis. For instance, to achieve a target precision of  $\varepsilon = 10^{-3}$ , the PAE with  $P = 64$  needs quantum circuits of depth 18 assisted by a 64-qubit GHZ state, demonstrating the ability of PAE to significantly reduce the circuit depth via parallelization.

We again emphasize that the main feature of PAE is its capability of controlling the trade-off between circuit depth and qubit count for the amplitude estimation. This may enable pursuing HL scaling for amplitude estimation even on depth-limited early fault-tolerant quantum computing devices. In addition, under the assumption that the wall-clock time of a quantum algorithm is determined by the depth of its quantum circuit, leveraging PAE to increase parallelism allows for a reduction in total computation time compared to conventional (non-parallel) methods.

Finally, we mention the arguments indicating that parallelization does not lead to speedup in Grover’s search algorithm [64] and approximate counting algorithm [65], both of which make essential use of the Grover operator, as does amplitude estimation. It is non-trivial to clarify the relevance of these arguments to our PAE, and this remains an open problem.

## ACKNOWLEDGMENTS

This work is supported by MEXT Quantum Leap Flagship Program Grant No. JPMXS0118067285 and JPMXS0120319794. K.O. acknowledges support by SIP Grant Number JPJ012367. K.W. was supported by JSPS KAKENHI Grant Number JP24KJ1963.

## APPENDIX

### A. CONSTRUCTION OF $V_{\varphi,T}$ WITH QSP

Using QSP,  $\tilde{V}_{\varphi,T}$  defined in Eq. (5) can be approximated as  $V_{\varphi,T}$  of the form:

$$V_{\varphi,T} = \prod_{l=1}^{L/2} (R_x(\xi'_{2l-1}) \otimes I_s) W_Q^\dagger (R_x(-\xi'_{2l-1}) \otimes I_s) \\ \times (R_x(\xi_{2l}) \otimes I_s) W_Q (R_x(-\xi_{2l}) \otimes I_s), \quad (A1)$$

where  $W_Q = cQ \times R_z(\pi/2)$ ,  $R_z(\xi) = e^{-i\xi Z_b/2}$  and  $R_x(\xi) = e^{-i\xi X_b/2}$ , with  $Z_b$  and  $X_b$  being the Pauli operators acting on the ancilla qubit.  $\vec{\xi}$  is a QSP hyperparameter, referred to as the angle sequence, chosen to ensure that  $V_{\varphi,T} \approx \tilde{V}_{\varphi,T}$ . Here,  $\xi' = \xi + \pi$ . The circuit structure of  $V_{\varphi,T}$  is illustrated in Fig. 3. The detail of this construction is presented in Supplemental Material Sec. S2

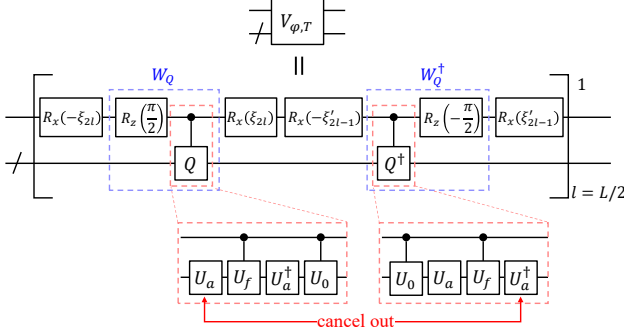


FIG. 3. Construction of  $V_{\varphi,T}$ . Here,  $L$  is a function of  $T$ , and  $\varphi$  is connected with the eigenphase  $2\theta$  of  $Q$  (in the Grover plane) by  $\varphi = 2\cos(2\theta)$ .

Note that  $U_a$  in  $W_Q$  cancels out with the adjacent  $U_a^\dagger$  in  $W_Q^\dagger$ . Therefore,  $V_{\varphi,T}$  contains a total of  $L$  applications of  $U_a$  and  $U_a^\dagger$ . To construct  $V_{\varphi,T}$ , it is also possible to employ the generalized QSP (GQSP) [66] instead of standard QSP. While GQSP has been shown to halve the cost of Hamiltonian simulation [67], it does not provide the same reduction in our setting, as the cancellation structure between  $U_a$  and  $U_a^\dagger$  does not arise when using GQSP.

### B. PSEUDOCODES

The complete PAE procedure and the classical post-processing in RPE are presented in Algorithms 1 and 2, respectively.

In PAE,  $P_k$  and  $T_k$  can be chosen under the constraint  $M_k = P_k T_k = 2^{k-1}$ , depending on available quantum resources. However, large  $T_k$  may destabilize the computation of the QSP hyperparameters [61, 68]. To ad-

dress this issue, one can achieve the same phase amplification effect by applying  $V_{\varphi,T}$  sequentially  $S$  times, at the cost of replacing  $\varepsilon_{\text{oc}} \mapsto S\varepsilon_{\text{oc}}$  in the error bound stated in Lemma 1 (see Supplemental Material Sec. S3 for details). Due to this error bound modification, the query complexity becomes  $N = \mathcal{O}(\varepsilon^{-1} + PS \log PS)$ , and the depth becomes  $\mathcal{O}(1/\varepsilon P + S \log PS)$ .

#### Algorithm 1 Parallel amplitude estimation

---

**Input:** Operator  $U_a, U_a^\dagger$ , target RMSE  $\varepsilon \in (0, 1)$ , target bias threshold  $\beta \in (0, \sqrt{6}/8)$ .

**Output:** Estimate  $\hat{a}$ .

- 1:  $K \leftarrow \lceil \log_2(1/\varepsilon) \rceil + 6$
- 2: Construct  $Q$  defined in Eq. (3) from  $U_a$  and  $U_a^\dagger$ .
- 3: Set  $[P_1, P_2, \dots, P_K]$  and  $[T_1, T_2, \dots, T_K]$  so that  $P_k T_k = 2^{k-1}, \forall k \in \{1, 2, \dots, K\}$ .
- 4: **for**  $k = 1, 2, \dots, K$  **do**  $\backslash\backslash$  This for-loop can be parallelized
- 5:    $\nu_k \leftarrow 1 + \lceil \log 6 \times (K - k)/2(\sqrt{6}/8 - \beta)^2 \rceil$
- 6:   Construct  $V_{\varphi,T_k}$  using  $U_a$  and  $U_a^\dagger$  for  $L_k = \mathcal{O}(T_k + \log(P_k/\beta))$  times.
- 7:   Perform  $V_{\varphi,T_k}^{\otimes P_k}$  on initial state  $|\text{GHZ}_{P_k}\rangle_b |0\rangle_s^{\otimes n P_k}$ , in the same manner as Fig. 1.
- 8:   Perform two measurements ( $\nu_k$  repetitions each):
  - (i) X-measurement on each ancilla qubit;
  - (ii) X-measurement on each ancilla qubit after applying  $e^{i\pi Z/4}$  to the first ancilla qubit.
- 9:   Set  $h_{+,k}$  and  $h_{i,k}$  to the counts of even-parity outcomes in cases (i) and (ii), respectively.
- 10:   Calculate  $f_{+,k} = h_{+,k}/\nu_k$  and  $f_{i,k} = h_{i,k}/\nu_k$ .
- 11: **end for**
- 12: Obtain  $\hat{a}$  using Algorithm 2 with  $\{f_{+,k}\}_{k=1}^K$  and  $\{f_{i,k}\}_{k=1}^K$ .

---

#### Algorithm 2 Robust phase estimation (classical post-processing part)

---

**Input:** Max. number of steps  $K$ , Observed probabilities  $\{f_{+,k}\}_{k=1}^K, \{f_{i,k}\}_{k=1}^K$

**Output:** Estimate  $\hat{\varphi} \in [-\pi, \pi]$

- 1: **for**  $k = 1, 2, \dots, K$  **do**
- 2:    $\widehat{M}_k \varphi'_k \leftarrow \text{atan2}(2f_{i,k} - 1, 2f_{+,k} - 1) \in [0, 2\pi)$
- 3:    $\hat{\varphi}'_{k,0} = \widehat{M}_k \varphi'_k / M_k \in [0, 2\pi/M_k]$ .
- 4:   **if**  $k = 1$  **then**
- 5:      $\hat{\varphi}'_1 \leftarrow \hat{\varphi}'_{1,0}$
- 6:   **else**
- 7:      $\eta \leftarrow \left\lfloor \frac{\hat{\varphi}'_{k-1}}{\pi/2^{k-2}} \right\rfloor$
- 8:     **if**  $\hat{\varphi}'_{k-1} - (\hat{\varphi}'_{k,0} + (\eta - 1)\pi/2^{k-2}) \leq \pi/2^{k-1}$  **then**
- 9:        $\hat{\varphi}'_k \leftarrow \hat{\varphi}'_{k,0} + (\eta - 1)\pi/2^{k-2}$
- 10:     **else if**  $(\hat{\varphi}'_{k,0} + (\eta + 1)\pi/2^{k-2}) - \hat{\varphi}'_{k-1} < \pi/2^{k-1}$  **then**
- 11:        $\hat{\varphi}'_k \leftarrow \hat{\varphi}'_{k,0} + (\eta + 1)\pi/2^{k-2}$
- 12:     **else**
- 13:        $\hat{\varphi}'_k \leftarrow \hat{\varphi}'_{k,0} + \eta\pi/2^{k-2}$
- 14:     **end if**
- 15:   **end if**
- 16:    $\hat{\varphi}_k \leftarrow \hat{\varphi}'_k - 2\pi \left\lfloor \frac{\hat{\varphi}'_k + \pi}{2\pi} \right\rfloor$
- 17: **end for**
- 18:  $\hat{\varphi} \leftarrow \hat{\varphi}_K$

---

---

[1] V. Giovannetti, S. Lloyd, and L. Maccone, Quantum metrology, *Phys. Rev. Lett.* **96**, 010401 (2006).

[2] V. Giovannetti, S. Lloyd, and L. Maccone, Advances in quantum metrology, *Nat. photonics* **5**, 222 (2011).

[3] E. Knill, G. Ortiz, and R. D. Somma, Optimal quantum measurements of expectation values of observables, *Phys. Rev. A—Atomic Molecular Optical Physics* **75**, 012328 (2007).

[4] S. Kimmel, G. H. Low, and T. J. Yoder, Robust calibration of a universal single-qubit gate set via robust phase estimation, *Phys. Rev. A* **92**, 062315 (2015).

[5] G. Wang, D. E. Koh, P. D. Johnson, and Y. Cao, Minimizing estimation runtime on noisy quantum computers, *PRX Quantum* **2**, 010346 (2021).

[6] A. Dutkiewicz, B. M. Terhal, and T. E. O’Brien, Heisenberg-limited quantum phase estimation of multiple eigenvalues with few control qubits, *Quantum* **6**, 830 (2022).

[7] Z. Ding and L. Lin, Even shorter quantum circuit for phase estimation on early fault-tolerant quantum computers with applications to ground-state energy estimation, *PRX Quantum* **4**, 020331 (2023).

[8] H. Ni, H. Li, and L. Ying, On low-depth algorithms for quantum phase estimation, *Quantum* **7**, 1165 (2023).

[9] K. Wada, K. Fukuchi, and N. Yamamoto, Quantum-enhanced mean value estimation via adaptive measurement, *Quantum* **8**, 1463 (2024).

[10] K. Oshio, Y. Suzuki, K. Wada, K. Hisanaga, S. Uno, and N. Yamamoto, Adaptive measurement strategy for noisy quantum amplitude estimation with variational quantum circuits, *Phys. Rev. A* **110**, 062423 (2024).

[11] K. Wada, N. Yamamoto, and N. Yoshioka, Heisenberg-limited adaptive gradient estimation for multiple observables, *PRX Quantum* **6**, 020308 (2025).

[12] G. Brassard, P. Hoyer, M. Mosca, and A. Tapp, Quantum amplitude amplification and estimation, *Contemp. Math.* **305**, 53 (2002).

[13] I. Kassal, S. P. Jordan, P. J. Love, M. Mohseni, and A. Aspuru-Guzik, Polynomial-time quantum algorithm for the simulation of chemical dynamics, *Proc. Natl. Acad. Sci.* **105**, 18681 (2008).

[14] L. Lin and Y. Tong, Near-optimal ground state preparation, *Quantum* **4**, 372 (2020).

[15] Y. Dong, L. Lin, and Y. Tong, Ground-state preparation and energy estimation on early fault-tolerant quantum computers via quantum eigenvalue transformation of unitary matrices, *PRX quantum* **3**, 040305 (2022).

[16] T. E. O’Brien, M. Streif, N. C. Rubin, R. Santagati, Y. Su, W. J. Huggins, J. J. Goings, N. Moll, E. Kyoseva, M. Degroote, C. S. Tautermann, J. Lee, D. W. Berry, N. Wiebe, and R. Babbush, Efficient quantum computation of molecular forces and other energy gradients, *Phys. Rev. Res.* **4**, 043210 (2022).

[17] P. Rebentrost, B. Gupt, and T. R. Bromley, Quantum computational finance: Monte carlo pricing of financial derivatives, *Phys. Rev. A* **98**, 022321 (2018).

[18] S. Woerner and D. J. Egger, Quantum risk analysis, *npj Quantum Inf.* **5**, 15 (2019).

[19] N. Stamatopoulos, D. J. Egger, Y. Sun, C. Zoufal, R. Iten, N. Shen, and S. Woerner, Option pricing using quantum computers, *Quantum* **4**, 291 (2020).

[20] N. Wiebe, A. Kapoor, and K. M. Svore, Quantum algorithms for nearest-neighbor methods for supervised and unsupervised learning, *Quantum Inf. Comput.* **15**, 316 (2015).

[21] N. Wiebe, A. Kapoor, and K. M. Svore, Quantum deep learning, *Quantum Inf. Comput.* **16**, 541 (2016).

[22] A. Kapoor, N. Wiebe, and K. Svore, Quantum perceptron models, *Adv. neural inf. process. syst.* **29** (2016).

[23] I. Kerenidis, J. Landman, A. Luongo, and A. Prakash, q-means: A quantum algorithm for unsupervised machine learning, *Adv. neural inf. process. syst.* **32** (2019).

[24] Y. Suzuki, S. Uno, R. Raymond, T. Tanaka, T. Onodera, and N. Yamamoto, Amplitude estimation without phase estimation, *Quantum Inf. Process.* **19**, 1 (2020).

[25] D. Grinko, J. Gacon, C. Zoufal, and S. Woerner, Iterative quantum amplitude estimation, *npj Quantum Inf.* **7**, 52 (2021).

[26] S. Aaronson and P. Rall, Quantum approximate counting, simplified, in *Symposium on simplicity in algorithms* (SIAM, 2020) pp. 24–32.

[27] K. Nakaji, Faster amplitude estimation, *Quantum Inf. Comput.* **20**, 1109 (2020).

[28] P. Intallura, G. Korpas, S. Chakraborty, V. Kungurtsev, and J. Marecek, A survey of quantum alternatives to randomized algorithms: Monte carlo integration and beyond, arXiv preprint arXiv:2303.04945 [10.48550/arXiv.2303.04945](https://arxiv.org/abs/2303.04945) (2023).

[29] F. Labib, B. D. Clader, N. Stamatopoulos, and W. J. Zeng, Quantum amplitude estimation from classical signal processing, arXiv preprint arXiv:2405.14697 [10.48550/arXiv.2405.14697](https://arxiv.org/abs/2405.14697) (2024).

[30] R. Cleve and J. Watrous, Fast parallel circuits for the quantum fourier transform, in *Proceedings 41st Annual Symposium on Foundations of Computer Science* (IEEE, 2000) pp. 526–536.

[31] C. Moore and M. Nilsson, Parallel quantum computation and quantum codes, *SIAM j. comput.* **31**, 799 (2001).

[32] P. Høyer and R. Špalek, Quantum fan-out is powerful, *Theory comput.* **1**, 81 (2005).

[33] P. Pham and K. M. Svore, A 2d nearest-neighbor quantum architecture for factoring in polylogarithmic depth, *Quantum Inf. Comput.* **13**, 937 (2013).

[34] J. Jiang, X. Sun, S.-H. Teng, B. Wu, K. Wu, and J. Zhang, Optimal space-depth trade-off of cnot circuits in quantum logic synthesis, in *Proceedings of the Fourteenth Annual ACM-SIAM Symposium on Discrete Algorithms* (SIAM, 2020) pp. 213–229.

[35] Z. Zhang, Q. Wang, and M. Ying, Parallel quantum algorithm for hamiltonian simulation, *Quantum* **8**, 1228 (2024).

[36] J. M. Martyn, Z. M. Rossi, K. Z. Cheng, Y. Liu, and I. L. Chuang, Parallel quantum signal processing via polynomial factorization, arXiv preprint arXiv:2409.19043 [10.48550/arXiv.2409.19043](https://arxiv.org/abs/2409.19043) (2024).

[37] Y. Quek, E. Kaur, and M. M. Wilde, Multivariate trace estimation in constant quantum depth, *Quantum* **8**, 1220 (2024).

[38] L. Cui, T. Schuster, F. Brandao, and H.-Y. Huang, Unitary designs in nearly optimal depth, arXiv preprint arXiv:2507.06216 (2025).

[39] T. Giurgica-Tiron, I. Kerenidis, F. Labib, A. Prakash,

and W. Zeng, Low depth algorithms for quantum amplitude estimation, *Quantum* **6**, 745 (2022).

[40] P. Rall and B. Fuller, Amplitude Estimation from Quantum Signal Processing, *Quantum* **7**, 937 (2023).

[41] D.-L. Vu, B. Cheng, and P. Rebentrost, Low-depth amplitude estimation without really trying, *ACM Trans. Quantum Comput.* **10.1145/3748666** (2025).

[42] G. H. Low and I. L. Chuang, Optimal hamiltonian simulation by quantum signal processing, *Phys. Rev. Lett.* **118**, 010501 (2017).

[43] D. Cruz, R. Fournier, F. Gremion, A. Jeannerot, K. Komagata, T. Tasic, J. Thiesbrummel, C. L. Chan, N. Macris, M.-A. Dupertuis, *et al.*, Efficient quantum algorithms for ghz and w states, and implementation on the ibm quantum computer, *Adv. Quantum Technol.* **2**, 1900015 (2019).

[44] G. J. Mooney, G. A. White, C. D. Hill, and L. C. Hollenberg, Generation and verification of 27-qubit greenberger-horne-zeilinger states in a superconducting quantum computer, *J. Phys. Commun.* **5**, 095004 (2021).

[45] J. I. Cirac, A. Ekert, S. F. Huelga, and C. Macchiavello, Distributed quantum computation over noisy channels, *Phys. Rev. A* **59**, 4249 (1999).

[46] A. Yimsiriwattana and S. J. Lomonaco Jr, Generalized ghz states and distributed quantum computing, arXiv preprint quant-ph/0402148 [10.48550/arXiv.quant-ph/0402148](https://arxiv.org/abs/10.48550/arXiv.quant-ph/0402148) (2004).

[47] R. Van Meter, K. Nemoto, W. Munro, and K. M. Itoh, Distributed arithmetic on a quantum multicomputer, *ACM SIGARCH Comput. Archit. News* **34**, 354 (2006).

[48] R. Beals, S. Brierley, O. Gray, A. W. Harrow, S. Kutin, N. Linden, D. Shepherd, and M. Stather, Efficient distributed quantum computing, *Proc. R. Soc. A: Math. Phys. Eng. Sci.* **469**, 20120686 (2013).

[49] M. Caleffi, M. Amoretti, D. Ferrari, J. Illiano, A. Manzalini, and A. S. Cacciapuoti, Distributed quantum computing: a survey, *Comput. Netw.* **254**, 110672 (2024).

[50] D. Barral, F. J. Cardama, G. Diaz-Camacho, D. Faïlde, I. F. Llovo, M. Mussa-Juane, J. Vázquez-Pérez, J. Vilasuso, C. Piñeiro, N. Costas, *et al.*, Review of distributed quantum computing: from single qpu to high performance quantum computing, *Comput. Sci. Rev.* **57**, 100747 (2025).

[51] G. H. Low and I. L. Chuang, Hamiltonian simulation by qubitization, *Quantum* **3**, 163 (2019).

[52] S. Uno, Y. Suzuki, K. Hisanaga, R. Raymond, T. Tanaka, T. Onodera, and N. Yamamoto, Modified grover operator for quantum amplitude estimation, *New J. Phys.* **23**, 083031 (2021).

[53] M. Braun, T. Decker, N. Hegemann, and S. Kersman, Error resilient quantum amplitude estimation from parallel quantum phase estimation, arXiv preprint arXiv:2204.01337 [10.48550/arXiv.2204.01337](https://arxiv.org/abs/10.48550/arXiv.2204.01337) (2022).

[54] G. H. Low, *Quantum signal processing by single-qubit dynamics*, Ph.D. thesis, Massachusetts Institute of Technology (2017).

[55] J. M. Martyn, Z. M. Rossi, A. K. Tan, and I. L. Chuang, Grand unification of quantum algorithms, *PRX quantum* **2**, 040203 (2021).

[56] A. Gilyén, S. Arunachalam, and N. Wiebe, Optimizing quantum optimization algorithms via faster quantum gradient computation, in *Proceedings of the Thirtieth Annual ACM-SIAM Symposium on Discrete Algorithms* (SIAM, 2019) pp. 1425–1444.

[57] B. Higgins, D. Berry, S. Bartlett, M. Mitchell, H. Wiseman, and G. Pryde, Demonstrating heisenberg-limited unambiguous phase estimation without adaptive measurements, *New J. Phys.* **11**, 073023 (2009).

[58] F. Belliardo and V. Giovannetti, Achieving heisenberg scaling with maximally entangled states: An analytic upper bound for the attainable root-mean-square error, *Phys. Rev. A* **102**, 042613 (2020).

[59] M. A. Nielsen and I. L. Chuang, *Quantum computation and quantum information* (Cambridge university press, 2010).

[60] A. Javadi-Abhari, M. Treinish, K. Krsulich, C. J. Wood, J. Lishman, J. Gacon, S. Martiel, P. D. Nation, L. S. Bishop, A. W. Cross, B. R. Johnson, and J. M. Gambetta, *Quantum computing with Qiskit* (2024), arXiv:2405.08810 [quant-ph].

[61] R. Chao, D. Ding, A. Gilyen, C. Huang, and M. Szegedy, Finding angles for quantum signal processing with machine precision, arXiv preprint arXiv:2003.02831 [10.48550/arXiv.2003.02831](https://arxiv.org/abs/10.48550/arXiv.2003.02831) (2020).

[62] <https://github.com/alibaba-edu/angle-sequence>.

[63] Y. Koizumi, K. Wada, W. Mizukami, and N. Yoshioka, Comprehensive study on heisenberg-limited quantum algorithms for multiple observables estimation, arXiv preprint arXiv:2505.00698 [10.48550/arXiv.2505.00698](https://arxiv.org/abs/10.48550/arXiv.2505.00698) (2025).

[64] C. Zalka, Grover’s quantum searching algorithm is optimal, *Phys. Rev. A* **60**, 2746 (1999).

[65] P. Burchard, Lower bounds for parallel quantum counting, arXiv preprint arXiv:1910.04555 [10.48550/arXiv.1910.04555](https://arxiv.org/abs/10.48550/arXiv.1910.04555) (2019).

[66] D. Motlagh and N. Wiebe, Generalized quantum signal processing, *PRX Quantum* **5**, 020368 (2024).

[67] D. W. Berry, D. Motlagh, G. Pantaleoni, and N. Wiebe, Doubling the efficiency of hamiltonian simulation via generalized quantum signal processing, *Phys. Rev. A* **110**, 012612 (2024).

[68] J. Haah, Product decomposition of periodic functions in quantum signal processing, *Quantum* **3**, 190 (2019).

## SUPPLEMENTAL MATERIAL

### S1. COMPARISON WITH OTHER QAE

Table S1 summarizes the comparison of PAE with prior QAEs in terms of the number of qubits, maximum circuit depth, and query complexity. Here,  $n$  denotes the number of qubits on which  $U_a$  acts.  $\varepsilon_{\text{add}}$  represents the additive error, whereas  $\varepsilon$  denotes the root mean squared error (RMSE).

Algorithm	#qubits	Max depth	#Query
QAE [12]	$n + \mathcal{O}(\log(1/\varepsilon_{\text{add}}))$	$\mathcal{O}\left(\frac{1}{\varepsilon_{\text{add}}}\right)$	$\mathcal{O}\left(\frac{1}{\varepsilon_{\text{add}}}\right)$
MLAE [24]	$n$	$\mathcal{O}\left(\frac{1}{\varepsilon}\right)$	$\mathcal{O}\left(\frac{1}{\varepsilon}\right)$
IQAE [25]	$n$	$\mathcal{O}\left(\frac{1}{\varepsilon_{\text{add}}}\right)$	$\mathcal{O}\left(\frac{1}{\varepsilon_{\text{add}}}\right)$
Power-law AE [39]	$n$	$\mathcal{O}\left(\frac{1}{\varepsilon_{\text{add}}^{1-\kappa}}\right)$	$\tilde{\mathcal{O}}\left(\frac{1}{\varepsilon_{\text{add}}^{1+\kappa}}\right)$
PAE(general) [This work]	$P(n+1)$	$\mathcal{O}\left(\frac{1}{P\varepsilon} + \log P\right)$	$\mathcal{O}\left(\frac{1}{\varepsilon} + P \log P\right)$
PAE(fully parallel) [This work]	$\mathcal{O}(n/\varepsilon)$	$\mathcal{O}\left(\log\left(\frac{1}{\varepsilon}\right)\right)$	$\mathcal{O}\left(\frac{\log(1/\varepsilon)}{\varepsilon}\right)$

TABLE S1. A comparison of QAE algorithms in terms of the number of qubits, maximum circuit depth, and query complexity. Here,  $n$  denotes the number of qubits acted on by  $U_a$ ,  $\varepsilon_{\text{add}}$  represents the additive estimation error, and  $\varepsilon$  denotes the RMSE. For the methods [12, 25, 39], the complexity is evaluated such that the final estimate has an additive error  $\varepsilon_{\text{add}}$  in a high probability. The parameter  $P$  is the degree of the parallelization in PAE, and  $\kappa \in (0, 1)$  controls the trade-off between circuit depth and query complexity in power-law AE. For simplicity, we ignore a log-log factor in IQAE.

The “fully parallel” variant of PAE achieves  $\mathcal{O}(\log(1/\varepsilon))$ -depth at the cost of increased qubit resources. To the best of our knowledge, PAE is the only method that achieves logarithmic depth scaling while maintaining query complexity at nearly Heisenberg limit (HL) scaling uniformly for all  $a \in [0, 1]$ .

### S2. CONSTRUCTION OF ENGINEERED PHASE SHIFTER WITH QSP

In this section, we explain how to construct the engineered phase shifter  $V_{\varphi, T}$  using quantum signal processing (QSP). First, we briefly review QSP, and then describe the procedure for constructing  $V_{\varphi, T}$ .

#### A. Overview of QSP

Given a unitary operator  $W = \sum_{\lambda} e^{i\theta_{\lambda}} |\lambda\rangle\langle\lambda|_s$ , QSP transforms the eigenphases  $\theta_{\lambda}$  in  $W$  by interleaving applications of the controlled operator  $W_x$ :

$$W_x := |+\rangle\langle+|_b \otimes I_s + |-\rangle\langle-|_b \otimes W, \quad (\text{S1})$$

and  $R_z(\xi)$  [42, 51, 54]. This results in the operator  $V_{x,\vec{\xi}}$

$$\begin{aligned} V_{x,\vec{\xi}} &= V_{x,\xi_1+\pi}^\dagger V_{x,\xi_2} \cdots V_{x,\xi_{L-1}+\pi}^\dagger V_{x,\xi_L} \\ &= \sum_{\lambda} (\mathcal{A}(\theta_{\lambda})I_b + i\mathcal{B}(\theta_{\lambda})Z_b + i\mathcal{C}(\theta_{\lambda})X_b + i\mathcal{D}(\theta_{\lambda})Y_b) \otimes |\lambda\rangle\langle\lambda|_s \\ &= \sum_{\lambda} \begin{pmatrix} \mathcal{A}(\theta_{\lambda}) + i\mathcal{B}(\theta_{\lambda}) & i\mathcal{C}(\theta_{\lambda}) + \mathcal{D}(\theta_{\lambda}) \\ i\mathcal{C}(\theta_{\lambda}) - \mathcal{D}(\theta_{\lambda}) & \mathcal{A}(\theta_{\lambda}) - i\mathcal{B}(\theta_{\lambda}) \end{pmatrix}_b \otimes |\lambda\rangle\langle\lambda|_s, \end{aligned} \quad (\text{S2})$$

$$V_{x,\xi} = (R_z(\xi) \otimes I_s) W_x (R_z(-\xi) \otimes I_s) \quad (\text{S3})$$

where  $L$  is an even integer,  $I_s$  and  $I_b$  denote the identity operators on the system and ancilla qubits, respectively.  $X_b, Y_b, Z_b$  are the Pauli operators acting on the ancilla qubit.  $\mathcal{A}, \mathcal{B}, \mathcal{C}$  and  $\mathcal{D}$  are real-valued functions determined by the rotation angles  $\vec{\xi} = (\xi_1, \dots, \xi_L)$ . The  $2 \times 2$  matrix in the rightmost equation acts on the computational basis  $\{|0\rangle_b, |1\rangle_b\}$  of the ancilla qubit.

The aforementioned construction of QSP using  $W_x$  and  $R_z(\xi)$  is referred to as the Wx-convention. An alternative form, known as the Wz-convention [55, 61], uses the operator  $W_z$ :

$$W_z := |0\rangle\langle 0|_b \otimes I_s + |1\rangle\langle 1|_b \otimes W, \quad (\text{S4})$$

and  $R_x(\xi)$ . Since the Wz-convention is well suited for constructing  $V_{\varphi,T}$  that induces a relative phase  $e^{iT\varphi}$  between  $|0\rangle$  and  $|1\rangle$ , we adopt it. In the  $W_z$ -convention, the operator  $V_{z,\vec{\xi}}$ , which is related to  $V_{x,\vec{\xi}}$ , satisfies the following [55]:

$$\begin{aligned} V_{z,\vec{\xi}} &= H_b V_{x,\vec{\xi}} H_b \\ &= \sum_{\lambda} \begin{pmatrix} \mathcal{A}(\theta_{\lambda}) + i\mathcal{C}(\theta_{\lambda}) & i\mathcal{B}(\theta_{\lambda}) - \mathcal{D}(\theta_{\lambda}) \\ i\mathcal{B}(\theta_{\lambda}) + \mathcal{D}(\theta_{\lambda}) & \mathcal{A}(\theta_{\lambda}) - i\mathcal{C}(\theta_{\lambda}) \end{pmatrix}_b \otimes |\lambda\rangle\langle\lambda|_s, \end{aligned} \quad (\text{S5})$$

where  $H_b$  is the Hadamard gate acting on the ancilla qubit. As will be shown later, to realize the required transformation, we only need to focus on  $(\mathcal{A}, \mathcal{C})$ . The theorem below holds for  $(\mathcal{A}, \mathcal{C})$ .

**Theorem 2 (Achievable  $(\mathcal{A}, \mathcal{C})$  in QSP - Theorem 1 of [42]).** *For all even integers  $L > 0$ , a pair of real functions  $\mathcal{A}, \mathcal{C}$  can be implemented by some angle sequence  $\vec{\xi} \in \mathbb{R}^L$  if and only if the following conditions are satisfied:*

- (1)  $\forall \theta \in \mathbb{R}, \mathcal{A}^2(\theta) + \mathcal{C}^2(\theta) \leq 1$
- (2)  $\mathcal{A}(0) = 1$
- (3)  $\mathcal{A}(\theta) = \sum_{l=0}^{L/2} a_l \cos(l\theta)$
- (4)  $\mathcal{C}(\theta) = \sum_{l=0}^{L/2} c_l \sin(l\theta)$

Moreover,  $\vec{\xi}$  can be computed from  $\mathcal{A}(\theta)$  and  $\mathcal{C}(\theta)$  in time  $\mathcal{O}(\text{poly}(L))$ .

## B. Detail of operator transformation with QSP

We now detail the construction of the approximate phase shifter  $V_{\varphi,T}$  using QSP. As the operator  $W_z$ , we employ  $W_Q$ :

$$\begin{aligned} W_Q &= cQ \times R_z(\pi/2) \\ &= \sum_{\sigma \in \{+, -\}} e^{i\theta_{Q\sigma}/2} \begin{pmatrix} e^{-i\theta_{Q\sigma}/2} & 0 \\ 0 & e^{i\theta_{Q\sigma}/2} \end{pmatrix}_b \otimes |Q_{\sigma}\rangle\langle Q_{\sigma}|_s, \end{aligned} \quad (\text{S6})$$

where  $\theta_{Q\pm} = \mp 2\theta + \pi/2$ , and we omit terms that act outside of the Grover plane, the same as  $cQ$ . To approximate  $\tilde{V}_{\varphi,T}$  defined in Eq. (5), it suffices to construct  $V_{z,\vec{\xi}}$  such that

$$\mathcal{A}(\theta_{Q\sigma}, T) \pm i\mathcal{C}(\theta_{Q\sigma}, T) = e^{\mp iT \sin \theta_{Q\sigma}} = e^{\mp iT \cos(2\theta)}, \quad (\text{S7})$$

where  $\sigma \in \{+, -\}$ . As demonstrated in Ref. [42],  $e^{\mp iT \sin \theta_{Q\sigma}}$  can be expanded by Bessel functions:

$$e^{\mp iT \sin \theta_{Q\sigma}} = J_0(T) + 2 \sum_{l \text{ even} > 0}^{\infty} J_l(T) \cos(l\theta_{Q\sigma}) \mp 2i \sum_{l \text{ odd} > 0}^{\infty} J_l(T) \sin(l\theta_{Q\sigma}). \quad (\text{S8})$$

We define  $\tilde{A}(\theta_{Q_\sigma}, T)$  and  $\tilde{C}(\theta_{Q_\sigma}, T)$  as following:

$$\tilde{A}(\theta_{Q_\sigma}, T) = J_0(T) + 2 \sum_{l \text{ even} > 0}^{L/2} J_l(T) \cos(l\theta_{Q_\sigma}), \quad i\tilde{C}(\theta_{Q_\sigma}, T) = 2i \sum_{l \text{ odd} > 0}^{L/2} J_l(T) \sin(l\theta_{Q_\sigma}). \quad (\text{S9})$$

Although  $\tilde{A}$  and  $\tilde{C}$  may not satisfy conditions (1) and/or (2) in Theorem 2, they can be approximated by feasible functions  $A$  and  $C$  which satisfy these conditions [42, 51]. Therefore, we can construct  $V_{z, \xi}$  such that  $\mathcal{A}(\theta_{Q_\sigma}, T) = A(\theta_{Q_\sigma}, T)$  and  $\mathcal{C}(\theta_{Q_\sigma}, T) = C(\theta_{Q_\sigma}, T)$ , where  $A(\theta_{Q_\sigma}, T) \pm iC(\theta_{Q_\sigma}, T) \approx e^{\mp iT \sin \theta_{Q_\sigma}} = e^{\mp iT \cos(2\theta)}$ .

Based on the above discussion, we can construct the operator  $V_{\varphi, T}$ :

$$\begin{aligned} V_{\varphi, T} &= \prod_{l=1}^{L/2} (R_x(\xi_{2l-1} + \pi) \otimes I_s) W_Q^\dagger (R_x(-\xi_{2l-1} - \pi) \otimes I_s) (R_x(\xi_{2l}) \otimes I_s) W_Q (R_x(-\xi_{2l}) \otimes I_s) \\ &= \sum_{\sigma \in \{+, -\}} \begin{pmatrix} A(\theta_{Q_\sigma}, T) + iC(\theta_{Q_\sigma}, T) & iB(\theta_{Q_\sigma}, T) - D(\theta_{Q_\sigma}, T) \\ iB(\theta_{Q_\sigma}, T) + D(\theta_{Q_\sigma}, T) & A(\theta_{Q_\sigma}, T) - iC(\theta_{Q_\sigma}, T) \end{pmatrix}_b \otimes |Q_\sigma\rangle \langle Q_\sigma|_s \\ &\approx \begin{pmatrix} e^{-iT \cos(2\theta)} & 0 \\ 0 & e^{iT \cos(2\theta)} \end{pmatrix}_b \otimes \bar{I}_s \\ &= \begin{pmatrix} e^{-iT \varphi/2} & 0 \\ 0 & e^{iT \varphi/2} \end{pmatrix}_b \otimes \bar{I}_s, \end{aligned} \quad (\text{S10})$$

where  $\varphi = 2 \cos(2\theta) = 2(1 - 2a)$ ,  $\bar{I}_s$  is the identity operator on the Grover plane, and terms acting outside the Grover plane are again omitted. Since  $(A, B, C, D)$  satisfies  $A^2 + B^2 + C^2 + D^2 = 1$  [54], the condition  $A(\theta_{Q_\sigma}, T) \pm iC(\theta_{Q_\sigma}, T) \approx e^{\mp iT \sin \theta_{Q_\sigma}}$  leads to  $|iB(\theta_{Q_\sigma}) \pm D(\theta_{Q_\sigma})| \approx 0$ .

### S3. PROOF OF QUERY COMPLEXITY FOR CONSTRUCTING $V_{\varphi, T}$

Here, we provide the detailed proof of Lemma 1 and the effect of the approximation error in  $V_{\varphi, T}$  when it is applied  $S$  times sequentially instead of increasing  $T$ .

**Lemma 1** (Query complexity for constructing  $V_{\varphi, T}$ ). *For any oracle conversion error  $\varepsilon_{\text{oc}} \in (0, 1)$ , there exists a quantum algorithm that constructs an operator  $V_{\varphi, T}$  such that  $\left\| (V_{\varphi, T} - \tilde{V}_{\varphi, T}) |j\rangle_b |0\rangle_s^{\otimes n} \right\| < \varepsilon_{\text{oc}}$ , using  $cQ$  and  $cQ^\dagger$  a total of  $L = \mathcal{O}(T + \log(1/\varepsilon_{\text{oc}}))$  times.*

*Proof of Lemma 1.* As shown in Supplemental Material Sec. S2, using QSP, we can construct  $V_{\varphi, T}$  that approximates  $\tilde{V}_{\varphi, T}$ . The construction of  $V_{\varphi, T}$  involves two approximations. The first is the approximation of  $e^{\mp iT \sin \theta_{Q_\sigma}}$  by the  $L/2$ -order Fourier series  $\tilde{A} \pm i\tilde{C}$ , as defined in Eq. (S9). The error caused by this approximation is upper-bounded as follows for any  $\theta_{Q_\sigma}$  [42]:

$$\left| \tilde{A}(\theta_{Q_\sigma}, T) \pm i\tilde{C}(\theta_{Q_\sigma}, T) - e^{\mp iT \sin \theta_{Q_\sigma}} \right| \leq \delta \leq \frac{4T^{L/2+1}}{2^{L/2+1} (L/2 + 1)!} \quad (\text{S11})$$

$$\begin{aligned} &< \frac{4}{e^{1/(6L+13)} \sqrt{2\pi(L/2 + 1)}} \left( \frac{eT}{L+2} \right)^{L/2+1} \\ &< 1.1 \left( \frac{eT}{L+2} \right)^{L/2+1}, \end{aligned} \quad (\text{S12})$$

where  $\sigma \in \{+, -\}$ , and we use Stirling's approximation  $(L/2 + 1)! > e^{1/(6L+13)} \sqrt{2\pi(L/2 + 1)} \left( \frac{L/2+1}{e} \right)^{L/2+1}$ . In the following discussion, we assume  $\delta \in (0, 1)$  and  $(eT/(L+2))^{L/2+1} \in (0, 1]$ . The second approximation is the replacement of  $\tilde{A}$  and  $\tilde{C}$  with achievable functions  $A$  and  $C$ , which satisfy the following inequality for any  $\theta_{Q_\sigma}$  [42].

$$|A(\theta_{Q_\sigma}, T) \pm iC(\theta_{Q_\sigma}, T) - e^{\mp iT \sin \theta_{Q_\sigma}}| \leq 8\delta. \quad (\text{S13})$$

Here, we express  $V_{\varphi,T}$  as following:

$$\begin{aligned} V_{\varphi,T} &= \sum_{\sigma \in \{+,-\}} \begin{pmatrix} A(\theta_{Q_\sigma}, T) + iC(\theta_{Q_\sigma}, T) & iB(\theta_{Q_\sigma}, T) - D(\theta_{Q_\sigma}, T) \\ iB(\theta_{Q_\sigma}, T) + D(\theta_{Q_\sigma}, T) & A(\theta_{Q_\sigma}, T) - iC(\theta_{Q_\sigma}, T) \end{pmatrix}_b \otimes |Q_\sigma\rangle\langle Q_\sigma|_s \\ &:= \sum_{\sigma \in \{+,-\}} \begin{pmatrix} \mathcal{F}_{0,\sigma,T} & i\mathcal{G}_{0,\sigma,T} \\ i\mathcal{G}_{1,\sigma,T} & \mathcal{F}_{1,\sigma,T} \end{pmatrix}_b \otimes |Q_\sigma\rangle\langle Q_\sigma|_s. \end{aligned} \quad (\text{S14})$$

Based on the above, the following inequality holds:

$$\begin{aligned} \left\| (V_{\varphi,T} - \tilde{V}_{\varphi,T}) |j\rangle_b |Q_\sigma\rangle_s \right\| &= \left\| (\mathcal{F}_{j,\sigma,T} - e^{(-1)^{j+1}iT \sin \theta_{Q_\sigma}}) |j\rangle_b + i\mathcal{G}_{j',\sigma,T} |j'\rangle_b \right\| \\ &\leq |\mathcal{F}_{j,\sigma,T} - e^{iT \phi_j}| + |\mathcal{G}_{j',\sigma,T}| \\ &< 8\delta + \sqrt{16\delta - 64\delta^2}, \end{aligned} \quad (\text{S15})$$

where  $j' \in \{0, 1\}$ ,  $j' \neq j$ , and  $(-1)^{j+1} \sin \theta_{Q_\sigma} = (-1)^{j+1} \cos 2\theta := \phi_j$ . To derive the rightmost inequality, we use the following relations:

$$\begin{aligned} 1 - |\mathcal{F}_{j,\sigma,T}| &\leq |\mathcal{F}_{j,\sigma,T} - e^{iT \phi_j}| \leq 8\delta, \\ \implies 1 - 8\delta &\leq |\mathcal{F}_{j,\sigma,T}|, \end{aligned} \quad (\text{S16})$$

$$\begin{aligned} |\mathcal{F}_{j,\sigma,T}|^2 + |\mathcal{G}_{j',\sigma,T}|^2 &= 1, \\ \implies |\mathcal{G}_{j',\sigma,T}| &\leq \sqrt{16\delta - 64\delta^2}. \end{aligned} \quad (\text{S17})$$

From Eq. (S15), the following inequality holds:

$$\begin{aligned} \left\| (V_{\varphi,T} - \tilde{V}_{\varphi,T}) |j\rangle_b |0\rangle_s^{\otimes n} \right\| &\leq \frac{1}{\sqrt{2}} \left( \left\| (V_{\varphi,T} - \tilde{V}_{\varphi,T}) |j\rangle_b |Q_+\rangle_s \right\| + \left\| (V_{\varphi,T} - \tilde{V}_{\varphi,T}) |j\rangle_b |Q_-\rangle_s \right\| \right) \\ &< \frac{2}{\sqrt{2}} \left( 8\delta + \sqrt{16\delta - 64\delta^2} \right) \end{aligned} \quad (\text{S18})$$

$$< 17\sqrt{\delta}, \quad (\text{S19})$$

Based on Eqs. (S12), (S19), to ensure that  $\left\| (V_{\varphi,T} - \tilde{V}_{\varphi,T}) |j\rangle_b |0\rangle_s^{\otimes n} \right\| \leq \varepsilon_{\text{oc}}$ , it suffices that  $18(eT/(L+2))^{L/4+1/2} \leq \varepsilon_{\text{oc}}$  holds. According to Ref. [56], this inequality is satisfied when  $L = e^2T + 4\log(18/\varepsilon_{\text{oc}}) - 2$ . Therefore, by setting  $L = e^2T + 4\log(1/\varepsilon_{\text{oc}}) + 10$  which exceeds the required threshold  $e^2T + 4\log(18/\varepsilon_{\text{oc}}) - 2$ , the inequality  $\left\| (V_{\varphi,T} - \tilde{V}_{\varphi,T}) |j\rangle_b |0\rangle_s^{\otimes n} \right\| < \varepsilon_{\text{oc}}$  holds.  $\blacksquare$

We now provide a proof of the following inequality presented in Appendix B: for any positive integer  $S$ ,

$$\left\| \left( V_{\varphi,T}^S - \tilde{V}_{\varphi,T}^S \right) |j\rangle_b |0\rangle_s^{\otimes n} \right\| < S\varepsilon_{\text{oc}}. \quad (\text{S20})$$

*Proof.* For  $\left\| \left( V_{\varphi,T}^S - \tilde{V}_{\varphi,T}^S \right) |j\rangle_b |0\rangle_s^{\otimes n} \right\|$ , the following inequality holds:

$$\left\| (V_{\varphi,T}^S - \tilde{V}_{\varphi,T}^S) |j\rangle_b |0\rangle_s^{\otimes n} \right\| = \left\| \sum_{k=0}^{S-1} V_{\varphi,T}^{S-k-1} \left( V_{\varphi,T} - \tilde{V}_{\varphi,T} \right) \tilde{V}_{\varphi,T}^k |j\rangle_b |0\rangle_s^{\otimes n} \right\| \quad (\text{S21})$$

$$\leq \sum_{k=0}^{S-1} \left\| V_{\varphi,T}^{S-k-1} \left( V_{\varphi,T} - \tilde{V}_{\varphi,T} \right) \tilde{V}_{\varphi,T}^k |j\rangle_b |0\rangle_s^{\otimes n} \right\|$$

$$= \sum_{k=0}^{S-1} \left\| \left( V_{\varphi,T} - \tilde{V}_{\varphi,T} \right) e^{ikT\phi_j} |j\rangle_b |0\rangle_s^{\otimes n} \right\|$$

$$= S \times \left\| (V_{\varphi,T} - \tilde{V}_{\varphi,T}) |j\rangle_b |0\rangle_s^{\otimes n} \right\| < S\varepsilon_{\text{oc}}. \quad (\text{S22})$$

$\blacksquare$

#### S4. CLASSICAL POST-PROCESSING IN ROBUST PHASE ESTIMATION

We describe the classical post-processing procedure of robust phase estimation (RPE) [4, 57, 58]. Throughout this section, we assume  $\varphi \in [-\pi, \pi]$  to describe the general RPE procedure, whereas PAE assumes  $\varphi \in [-2, 2]$ . Given the quantum circuit measurement outcomes  $\{f_{+,k}\}_{k=1}^K$  and  $\{f_{i,k}\}_{k=1}^K$ , the following procedure is executed for  $k = 1, 2, \dots, K$  to estimate  $\varphi$ . Hereafter,  $\varphi'$  and  $\hat{\varphi}'$  denote the values of  $\varphi$  and  $\hat{\varphi}$  mapped from  $[-\pi, \pi]$  to  $[0, 2\pi]$ .

1. Derive estimate  $\widehat{M_k \varphi'_k} := \text{atan2}(2f_{i,k} - 1, 2f_{+,k} - 1) \in [0, 2\pi]$ , where  $M_k = 2^{k-1}$ .
2. Calculate  $\hat{\varphi}'_{k,0} := \widehat{M_k \varphi'_k} / M_k \in [0, 2\pi/M_k]$ . As shown in Fig. S1,  $\hat{\varphi}'_{k,0}$  represents the smallest candidate for  $\hat{\varphi}'_k$  in the range  $[0, 2\pi]$ .
3. If  $k = 1$ , adopt  $\hat{\varphi}'_{0,1}$  as  $\hat{\varphi}'_1$ .
- If  $k > 1$ , select  $\hat{\varphi}'_k$  from the candidate estimates  $\{\hat{\varphi}'_{k,m} = \hat{\varphi}'_{k,0} + m\pi/2^{k-2}\}_{m=-1}^{2^{k-1}}$  based on the previous estimate  $\hat{\varphi}'_{k-1}$ . First, compute the partition index  $\eta := \lfloor \hat{\varphi}'_{k-1}/2^{-k+2}\pi \rfloor \in \{0, 1, \dots, 2^{k-1}-1\}$ , which identifies the partition in which  $\hat{\varphi}'_{k-1}$  lies (see Fig. S1). Then, select  $\hat{\varphi}'_k$  from the candidate estimates corresponding to the partition indices  $\eta - 1, \eta$ , and  $\eta + 1$  whose confidence intervals, defined as the estimate  $\pm\pi/3 \times 2^{k-1}$ , overlap with that of  $\hat{\varphi}'_{k-1}$ .
4. Map  $\hat{\varphi}'_k$  onto  $[-\pi, \pi]$  to obtain  $\hat{\varphi}_k$ .

The final estimate  $\hat{\varphi}$  is given by  $\hat{\varphi}_K$ . Figure S1 schematically illustrates the above estimation procedure.

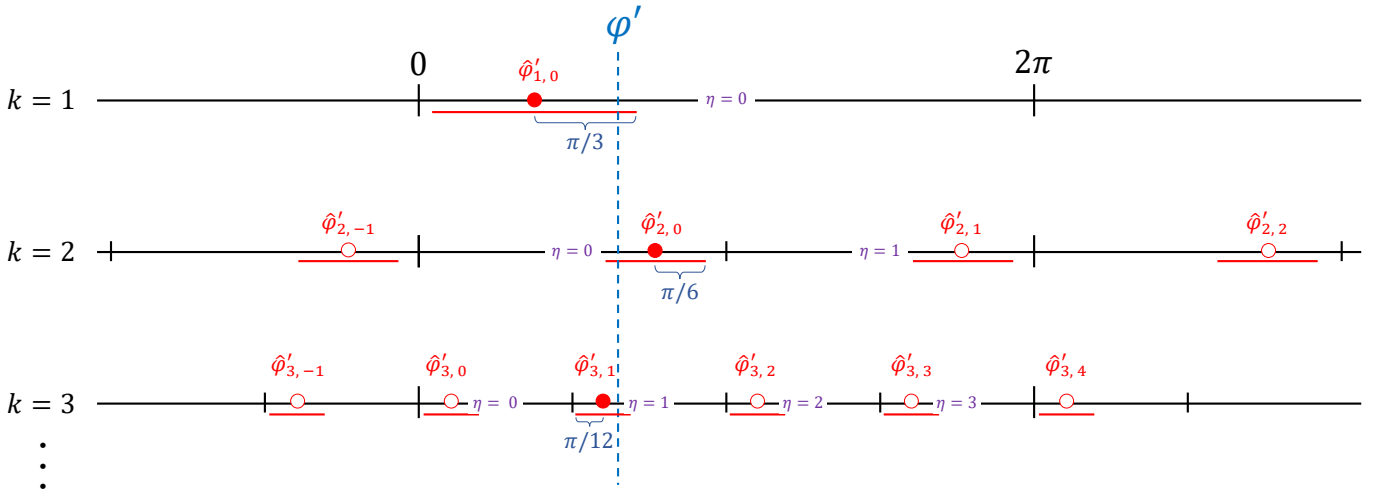


FIG. S1. Schematic diagram of the step-by-step estimation of  $\varphi$  in RPE. The filled red circles indicate the estimates adopted as  $\hat{\varphi}'_k$ , that is, in this example, we have  $\hat{\varphi}'_1 = \hat{\varphi}'_{1,0}$ ,  $\hat{\varphi}'_2 = \hat{\varphi}'_{2,0}$  and  $\hat{\varphi}'_3 = \hat{\varphi}'_{3,1}$ .

Below, we restate the pseudocode for the classical post-processing presented in Appendix B.

---

**Algorithm 2** Robust phase estimation (classical post-processing part)

---

**Input:** Max. number of steps  $K$ , Observed probabilities  $\{f_{+,k}\}_{k=1}^K, \{f_{i,k}\}_{k=1}^K$ 
**Output:** Estimate  $\hat{\varphi} \in [-\pi, \pi)$ 

```

1: for  $k = 1, 2, \dots, K$  do
2:    $M_k = 2^{k-1}$ 
3:    $\widehat{M_k \varphi'_k} \leftarrow \text{atan2}(2f_{i,k} - 1, 2f_{+,k} - 1) \in [0, 2\pi)$ 
4:    $\widehat{\varphi}'_{k,0} = \widehat{M_k \varphi'_k} / M_k \in [0, 2\pi/M_k)$ .
5:   if  $k = 1$  then
6:      $\widehat{\varphi}'_1 \leftarrow \widehat{\varphi}'_{1,0}$ 
7:   else
8:      $\eta \leftarrow \left\lfloor \frac{\widehat{\varphi}'_{k-1}}{\pi/2^{k-2}} \right\rfloor$ 
9:     if  $\widehat{\varphi}'_{k-1} - (\widehat{\varphi}'_{k,0} + (\eta - 1)\pi/2^{k-2}) \leq \pi/2^{k-1}$  then
10:       $\widehat{\varphi}'_k \leftarrow \widehat{\varphi}'_{k,0} + (\eta - 1)\pi/2^{k-2}$ 
11:    else if  $(\widehat{\varphi}'_{k,0} + (\eta + 1)\pi/2^{k-2}) - \widehat{\varphi}'_{k-1} < \pi/2^{k-1}$  then
12:       $\widehat{\varphi}'_k \leftarrow \widehat{\varphi}'_{k,0} + (\eta + 1)\pi/2^{k-2}$ 
13:    else
14:       $\widehat{\varphi}'_k \leftarrow \widehat{\varphi}'_{k,0} + \eta\pi/2^{k-2}$ 
15:    end if
16:   end if
17:    $\widehat{\varphi}_k \leftarrow \widehat{\varphi}'_k - 2\pi \left\lfloor \frac{\widehat{\varphi}'_k + \pi}{2\pi} \right\rfloor$ 
18: end for
19:  $\hat{\varphi} \leftarrow \widehat{\varphi}_K$ 

```

---

## S5. NUMERICAL EVALUATION OF THE APPROXIMATION ERROR IN $V_{\varphi,T}$ AND ITS IMPACT ON ESTIMATION

We numerically evaluated how the approximation error in  $V_{\varphi,T}$  affects the estimation error of  $a$ , and how this approximation error depends on the number of  $U_a$  and  $U_a^\dagger$  contained in  $V_{\varphi,T}$ .

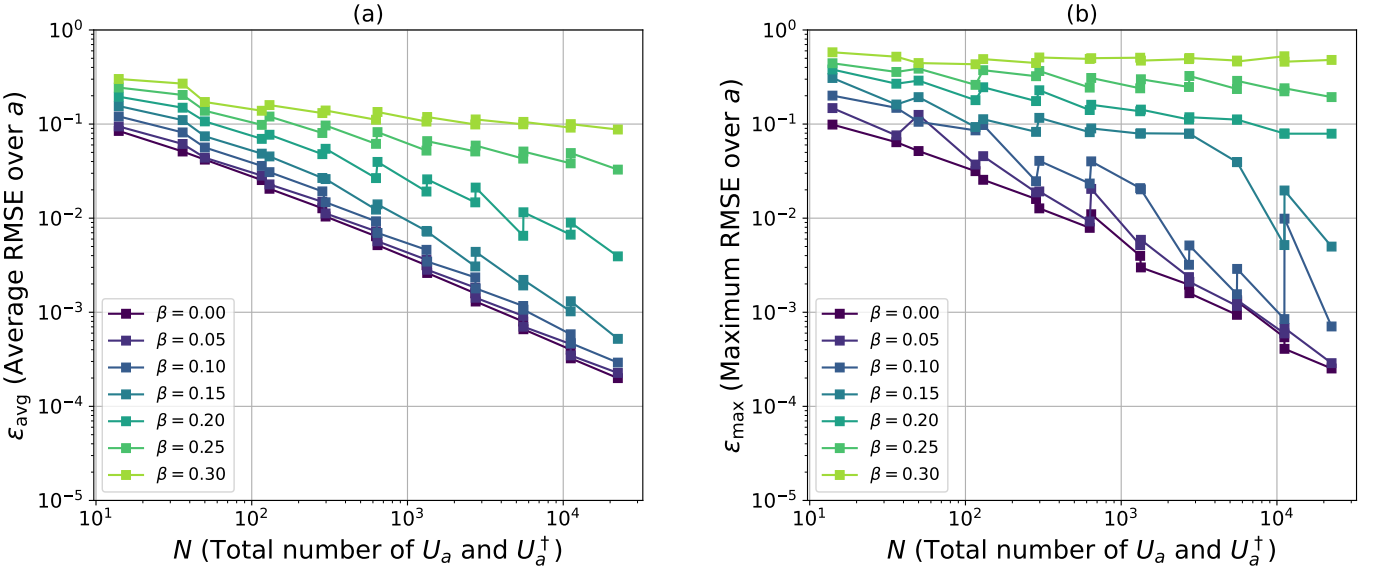


FIG. S2. The relationship between the number of queries to  $U_a$  and  $U_a^\dagger$ , and (a) the average value and (b) the maximum value of  $\varepsilon$  over  $a$ , as the parameter  $\beta$  varies.

First, we present a numerical evaluation of the relationship between  $\beta$ , the bias in the measurement probability, and the query complexity. Figure S2 shows the query complexity for various values of  $\beta \in \{0.00, 0.05, 1.00, 1.50, 2.00, 2.50, 3.00\}$ . In this experiment, we assume  $\beta_{+,k} = \beta_{i,k} = \beta$ . To compute  $N$ , we set  $L_k = 1$  for all  $k$ . We perform the estimation by sampling measurement outcomes according to the probability

$p_{+,k} = (1 + \cos M_k \varphi)/2 + \beta$  and  $p_{i,k} = (1 + \sin M_k \varphi)/2 + \beta$ . We evaluate  $\varepsilon$  by performing 100 estimation trials for each  $a \in \{0.00, 0.01, \dots, 1.00\}$ , and compute the average ( $\varepsilon_{\text{avg}}$ ) and maximum ( $\varepsilon_{\text{max}}$ ) values of  $\varepsilon$ . All other parameters are set as in the experiment presented in the main text, using  $\nu_k = \lfloor 4.0835(K - k) + \nu_K \rfloor$ ,  $\nu_K \in [7, 18]$ , and  $K \in \{1, 2, \dots, 9\}$ . Based on the result in Fig. S2, when  $\beta = 0.05$ , the estimation accuracy is comparable to that achieved when  $\beta = 0$ , even though the settings of  $\nu_k$  and  $\nu_K$  are the same (i.e., the bias is not taken into account when configuring these parameters).

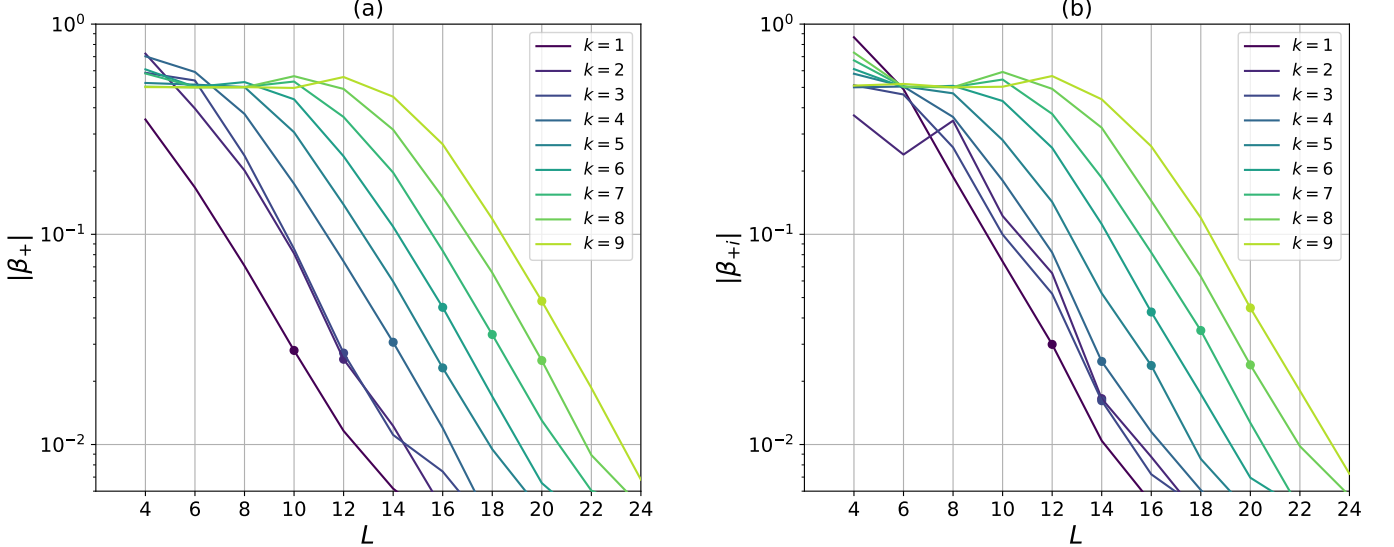


FIG. S3. The relationship of  $L \in \{2, 4, \dots, 24\}$  with (a)  $|\beta_{+,k}|$  and (b)  $|\beta_{i,k}|$ , for  $k \in \{1, 2, \dots, 9\}$ . Dots indicate the data points with the smallest  $L$  that satisfy  $|\beta_{+,k}| \leq 0.05$  and  $|\beta_{i,k}| \leq 0.05$  for each  $k$ .

Next, we present the results of a numerical evaluation of how the approximation error in  $V_{\varphi,T}$  affects  $\beta$ . In this experiment, we fix  $T = 1$ , and evaluate  $|\beta_{+,k}|$  and  $|\beta_{i,k}|$  for  $L \in \{4, 6, \dots, 24\}$  and  $K \in \{1, 2, \dots, 9\}$ .  $\beta_{+,k}$  and  $\beta_{i,k}$  are computed via quantum circuit simulation using Qiskit [60], where the measurement probabilities  $p_{+,k}$  and  $p_{i,k}$  are estimated from 100000-shot measurements. We calculate the angle sequence  $\vec{\xi}$  using the Python library [62], as in the experiment described in the main text. In Fig. S3,  $|\beta_{+,k}|$  and  $|\beta_{i,k}|$  are computed as the maximum values over  $a \in \{0.00, 0.01, \dots, 1.00\}$ . As shown in Fig. S3,  $|\beta_{+,k}|$  and  $|\beta_{i,k}|$  decrease exponentially as  $L$  increases for sufficiently large  $L$ . This observation is consistent with the behavior predicted by Lemma 1 and the inequality  $|\beta_{r,k}| \leq \sqrt{2}P_k \max_j \|(V_{\varphi,T_k} - \tilde{V}_{\varphi,T_k}) |j\rangle_b |0\rangle_s^{\otimes n}\|$  stated in the proof of Theorem 1. Figure S3 also shows that the condition  $|\beta_{+,k}|, |\beta_{i,k}| \leq 0.05$ , required to achieve accuracy comparable to the  $\beta = 0$  case as shown in Fig. S2, can be satisfied by setting  $(L_1, L_2, \dots, L_{13}) = (10, 12, 12, 14, 16, 16, 18, 20, 20)$  for X-basis measurement, and  $(L_1, L_2, \dots, L_{13}) = (12, 14, 14, 14, 16, 16, 18, 20, 20)$  for the other measurement. Accordingly, we adopt these values of  $L_k$  in the experiment presented in the main text.

We also evaluate  $L$  required to ensure  $\beta \leq 0.05$  in the full sequential case (i.e.  $P = 1, T = 2^{K-1}$ ). According to Eq. (S18) and the inequality  $|\beta_{r,k}| \leq \sqrt{2}P_k \max_j \|(V_{\varphi,T_k} - \tilde{V}_{\varphi,T_k}) |j\rangle_b |0\rangle_s^{\otimes n}\|$ , the condition  $\beta \leq 0.05$  is fulfilled if  $8\delta + \sqrt{16\delta - 64\delta^2} \leq 0.025$ , which holds when  $\delta < 3.813 \times 10^{-5}$ . From Eq. (S11), this constraint on  $\delta$  leads to the following condition on  $L$ :

$$\frac{4T^{L/2+1}}{2^{L/2+1}(L/2+1)!} < 3.813 \times 10^{-5}. \quad (\text{S23})$$

Figure S4 illustrates the  $T$ - $L$  relationship obtained by replacing the inequality sign ' $<$ ' in Eq. (S23) with the equality. Based on this result, we use  $(L_1, L_2, L_3, L_4) = (10, 14, 22, 34)$  in the numerical experiments described in the main text for the full sequential case. In addition, as shown in Fig. S4, a linear fit for  $T \geq 10$  yields  $L = 2.72T + 13.64$ . Therefore, we set  $L_k = 2 \lceil (2.72T_k + 13.64)/2 \rceil$  for  $k \geq 5$ .

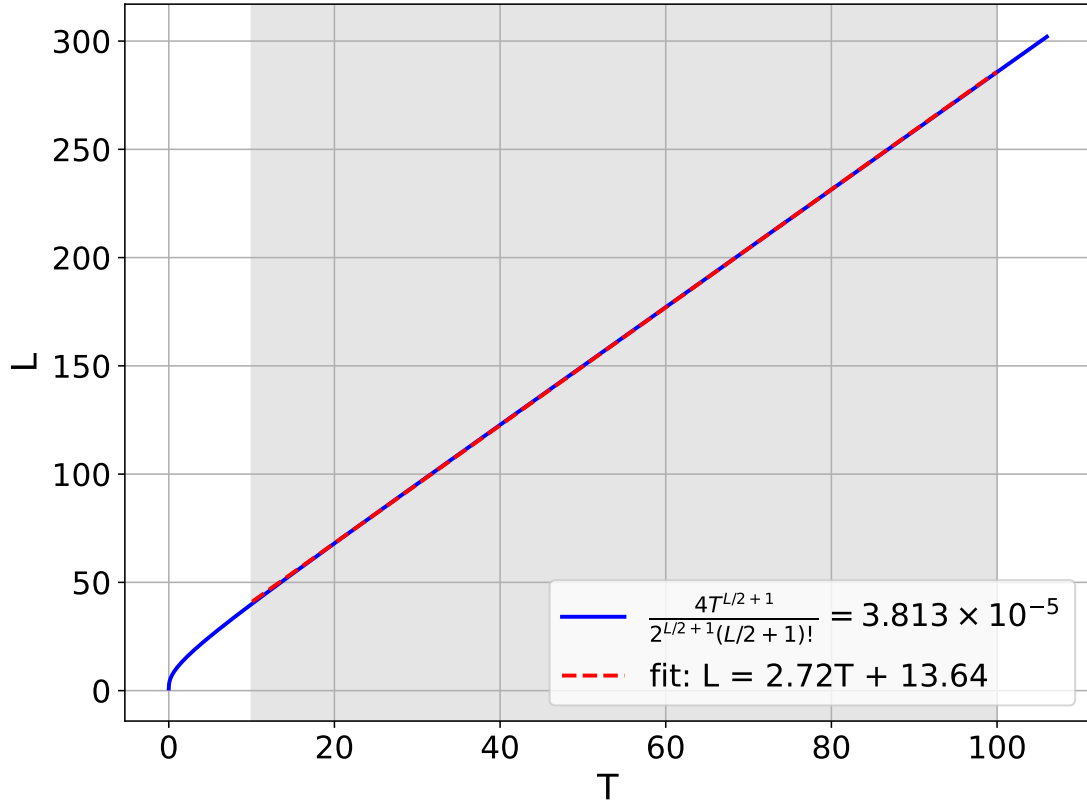


FIG. S4.  $T$ - $L$  relationship derived by replacing the inequality in Eq. (S23) with the equality. The blue line represents the resulting  $T$ - $L$  curve, while the red dashed line shows the linear fitting result for  $10 \leq T \leq 100$ .